Author(s): Hannula, Jari-Matti & Viikari, Ville

Title: Uncertainty analysis of intermodulation-based antenna measurements

Year: 2016

Version: Post print

Please cite the original version:

Hannula, Jari-Matti & Viikari, Ville. 2016. Uncertainty analysis of intermodulation-based antenna measurements. Proceedings of the 10th European Conference on Antennas and Propagation (EuCAP 2016). 5. DOI: 10.1109/eucap.2016.7481283.

Uncertainty Analysis of Intermodulation-Based Antenna Measurements

Jari-Matti Hannula and Ville Viikari

Department of Radio Science and Engineering, Aalto University, Espoo, Finland
Email: jari-matti.hannula@aalto.fi, ville.viikari@aalto.fi

***Abstract*—Intermodulation measurement principle has been proposed for characterizing transponder antennas. Although the method seems to offer certain advantages compared to traditional antenna characterization methods, the measurement uncertainty has not yet been well characterized. We aim at identifying the main sources of measurement uncertainty and estimating the achievable accuracy in a certain case at 1 GHz.**

***Index Terms*—antenna measurements, nonlinearity, transponders, uncertainty.**

I. Introduction

Wireless identification, sensing, and tracking is an increasingly important application of radio engineering. Used technologies include RFID [1], harmonic transponders [2], and various wireless sensors [3]. What these systems have in common is that they all operate using a nonlinear load connected to an electrically small antenna.

The effects of the measurement cable in measurements of electrically small antennas are well-known. The measurement cable easily becomes a part of the radiating structure, so instead of only the antenna, both the antenna and the environment are measured [4]. Techniques for avoiding these effects include the use of balun chokes to reduce the current induced to the measurement cable [5], [6].

Measurement methods that avoid the use of the cable can therefore be highly relevant. This is especially important in transponder applications that do not use any connecting cables during their normal operation. Instead, they are directly matched to the transponder chip, the impedance of which is often far away from the conventional 50-Ω level used by common RF measurement equipment.

The intermodulation measurement technique was introduced in [7] for RFID and was further developed in [8] to characterize harmonic transponders. It uses a nonlinear load to generate a response at the third-order intermodulation frequencies. Because of the inherent nonlinearity in transponders, the technique is well-suited for characterizing transponder antennas.

However, there has been no detailed analysis on the uncertainty of the measurement technique. In this paper we take a further look at the results of [8], define the sources of uncertainty and calculate the total uncertainty in the obtained results. Uncertainty analysis is needed to estimate the measurement accuracy which is important for comparing the intermodulation measurement technique with traditional antenna measurement techniques.

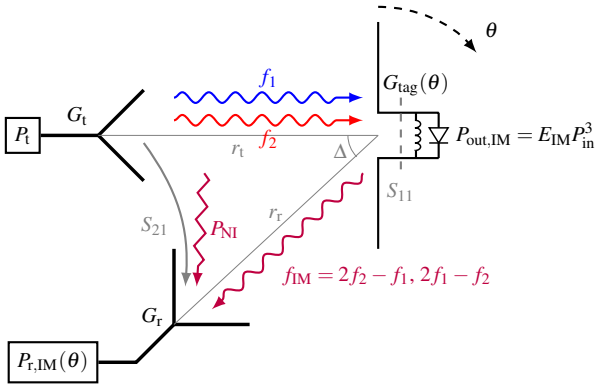

Fig. 1. The measurement principle analyzed in this paper. The AUT has a nonlinear load connected to it. It is then illuminated with two closely spaced frequencies, causing it to scatter back a response at intermodulation frequencies. The intermodulation response generated by the AUT is recorded and gain can be calculated by rotating the AUT.

II. Background

Fig. 1 illustrates the measurement setup used in the technique. The measurement is performed for the Antenna Under Test (AUT) that has a nonlinear load connected to it. The AUT is then illuminated with two closely located frequencies f_1 and f_2. Because of the nonlinearity, the transponder produces intermodulation products at $2f_2 - f_1$ and $2f_1 - f_2$. Either of these frequencies can be used. The selected frequency is denoted as f_{IM}.

The generated intermodulation response is then recorded and used to characterize the antenna. The analytical response has been derived in [8] and it is

$$P_{\mathrm{r,IM}} = \underbrace{P_{\mathrm{t}}^3 \frac{G_{\mathrm{t}}^3 G_{\mathrm{r}}}{r_{\mathrm{t}}^6 r_{\mathrm{r}}^2} \left(\frac{\lambda}{4\pi}\right)^8}_{\text{setup}} \underbrace{G_{\mathrm{tag}}^4 (1 - |S_{11}|^2)^4}_{\text{realized gain of antenna}} \underbrace{E_{\mathrm{IM}}}_{\substack{\text{mixing} \\ \text{element}}} \tag{1}$$

where $P_{\mathrm{r,IM}}$ is the received intermodulation response, P_{t} is the transmitter input power, G_{t} is the transmitter gain (including amplifier, cables, and transmitter antenna), G_{r} is the receiver gain, r_{t} and r_{r} are the AUT distances from the transmitter and the receiver, λ is the wavelength, G_{tag} is the transponder

antenna gain, $|S_{11}|$ is the magnitude of the reflection coefficient between the transponder antenna and the transponder load, and E_{IM} describes the intermodulation generation of the load $P_{\mathrm{out,IM}} = E_{\mathrm{IM}} P_{\mathrm{in}}^3$, where $P_{\mathrm{out,IM}}$ is the power generated by the transponder at the intermodulation frequency and P_{in} is the power accepted by the transponder at one fundamental frequency. These parameters are also illustrated in Fig. 1 that depicts the bistatic measurement setup. For more details on how the theory was formulated, see [8].

A. Gain Measurement

To characterize the antenna, the antenna properties can be solved from (1). We measure the realized gain, so the matching efficiency is included in the measured value. We define the realized gain in (1) as $G_{\mathrm{tag}}^4(1-|S_{11}|^2)^4 = G(\theta)^3 G(\theta+\Delta)$ with the angles θ and Δ as shown in Fig. 1

$$G(\theta)^3 G(\theta+\Delta) = \left(\frac{4\pi}{\lambda}\right)^8 \frac{r_{\mathrm{t}}^6 r_{\mathrm{r}}^2}{G_{\mathrm{t}}^3 G_{\mathrm{r}} E_{\mathrm{IM}} P_{\mathrm{t}}^3} P_{\mathrm{r,IM}}(\theta). \quad (2)$$

Only the received response $P_{\mathrm{r,IM}}$ depends on the AUT rotation angle. All the other parameters remain constant, and are from now on denoted using a parameter A. Using this notation, discretizing the measurement points, and converting the values to decibel scale, the gain at one single measurement point is

$$3G_i^3 + G_{i+\Delta} = A + P_i. \quad (3)$$

There are corresponding equations derived for different measurement configurations in [8, eqs. (17), (20), (21)]. The measurements were performed using the bistatic measurement geometry, which is why we focus on that configuration in this paper. In bistatic geometry the gain can be calculated from

$$\begin{pmatrix} G_1 \\ G_2 \\ \vdots \\ G_{n-1} \\ G_n \end{pmatrix} = \begin{pmatrix} 3 & \cdots & 1 & \cdots & 0 \\ 0 & 3 & \cdots & 1 & \vdots \\ \ddots & \ddots & \ddots & \ddots & \ddots \\ \vdots & 1 & \ddots & 3 & 0 \\ 0 & \cdots & 1 & \cdots & 3 \end{pmatrix}^{-1} \begin{pmatrix} A+P_{\mathrm{r},1} \\ A+P_{\mathrm{r},2} \\ \vdots \\ A+P_{\mathrm{r,n-1}} \\ A+P_{\mathrm{r,n}} \end{pmatrix} \quad (4)$$

which can be obtained by combining (3) into a linear system of equations for all $i = 1 \ldots n$.

Bistatic measurement geometry results in improved dynamic range compared to the monostatic measurement. However, the use of said geometry also adds some challenges to calculating the measured value. The gain cannot be calculated from only one measurement point, but the gain depends on the received response at several different angles. Each measurement point This effect depends on the offset Δ between the measurement antennas. If the offset is 180°, the gain at one point depends on two different measurement points. With an offset of 120° it depends on three, e.g. gain at 0° depends on the response measured at 0°, 120°, 240°. The same principle applies when the offset is made smaller.

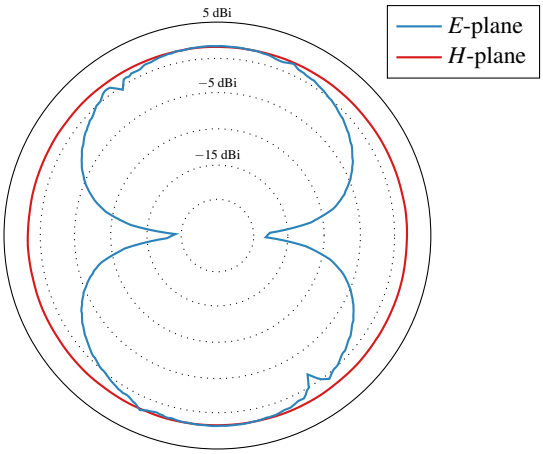

Fig. 2. An example of a measured radiation pattern of a harmonic transponder obtained using this technique. Result from [8].

III. Sources of Uncertainty

In this section, we characterize the sources of uncertainty in the measurement. The majority of the terms in the equation remain constant over the measurement. We can therefore separate the analysis into two separate cases: constant uncertainty that is present at all measured angles and the uncertainty that changes at each measurement point. The uncertainty analysis is performed for the gain pattern of a harmonic transponder at 1 GHz. Fig. 2 illustrates this result obtained in [8].

A. Static Variables

This section considers the measurement parameters related to the measurement setup itself, labeled "setup" in (1). It includes the uncertainty of the transmitter power P_{t}, accuracy of the measured response P_{r}, transmitter and receiver gains G_{t} and G_{r}, and the measurement distances r_{t} and r_{r}.

Transmitter and receiver gain and loss are measured with the spectrum analyzer. There is some standard error in the value measured by the spectrum analyzer which is easily found from the specifications of the device. Uncertainty before the intermodulation conversion is more significant than after because the terms at the fundamental frequencies in (1) have a larger effect than at the intermodulation frequency.

If the transmit and receive antennas are identical, the uncertainty of the measured gain is proportional to the uncertainty of the measurement antennas. The properties of the measurement antennas should therefore be well-known. In addition. the distance to the AUT should be measured from the phase center of the measurement antennas. The phase center varies somewhat depending on the frequency and can be difficult to pinpoint exactly. A larger source of uncertainty is the location of the phase center of the measurement antennas, which is not known exactly.

Another important factor related to the distance is the far-field assumption. The distance to the AUT has to be small to reduce the path loss but large enough that far-field conditions are met. Any near-field effects result in errors in the model.

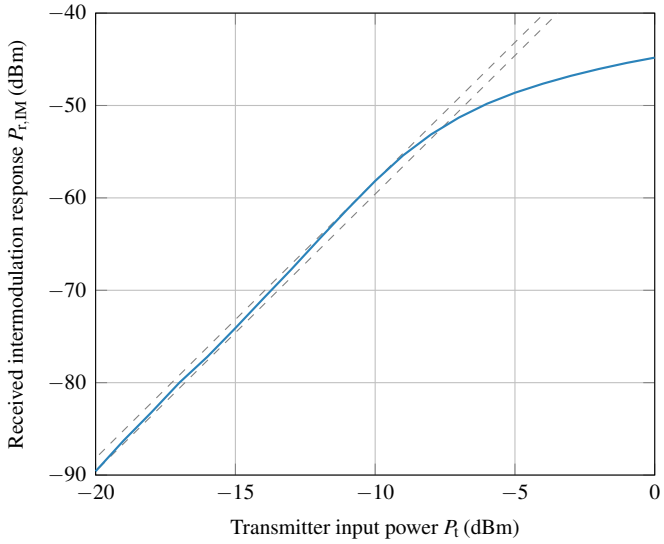

Fig. 3. The measured response as a function of transmit power.

The model assumes far-field propagation, i.e.

$$P_{\mathrm{r}} \sim \left(\frac{1}{kr}\right)^8 \tag{5}$$

where $k = 2\pi/\lambda$. In the near field, however, the field depends on various powers of the distance. In the worst case, there are three terms that contribute to the response. Assuming the worst case, the ratio between the power propagating in the far-field and near-field is [9, p. 27]

$$P_{\mathrm{rel}} = \frac{\left|\frac{1}{kr}\right|^8}{\left|\frac{1}{kr} + \frac{1}{k^2r^2} + \frac{1}{k^3r^3}\right|^8} \tag{6}$$

We also assume single-path line-of-sight propagation. We neglect multiple reflections in the present case because the measurements were performed in an anechoic chamber and attenuation due to distance is significant.

B. Power-dependent Variables

The measurement technique is nonlinear, which makes it important to consider the effects due to varying input power. A limitation in the bistatic setup is the variability of the input power. The multistatic setup of [7] would avoid this problem but we have used the bistatic setup due to the simpler mechanical construction. This requires that the input power of the system is adjusted iteratively based on the gain of the AUT.

The nonlinear load is modeled using the parameter E_{IM}, with the assumption that E_{IM} is constant. This approximation is accurate at low power levels. The small-signal model assumes that the intermodulation response is proportional to the third power of the input power. In reality, the relation is not exactly logarithmic. Fig. 3 illustrates this concept. When the transmitted power is smaller than -9 dBm, the error between the model and the measurement is less than 1.4 dB.

Common harmonic transponder designs include an inductance parallel to the diode [10], [11]. This provides a path for the generated dc current, preventing the operating point of the diode from changing. If there is no dc path in the nonlinear load, then the response can have a larger effect.

C. Angle-dependent Variables

In the ideal case, the response at the receiver depends on the direct propagation from the transmitter to the transponder, and then back to the receiver. Additionally, there is interference caused by noise and the distortion coupling from the transmitter to the receiver. It is also the one that causes the shape of the measured pattern to change because the error caused by the noise and the distortion depends on the level of the measured response. A significant problem is the low Signal-to-Interference-Plus-Noise-Ratio (SINR) near the nulls in the antenna pattern.

The total power of noise and interference picked up by the receiver is

$$P_{\mathrm{I}} = \frac{|S_{21}|^2 P_{\mathrm{t}}^3}{LOIP_{3,\mathrm{t}}^2} + \frac{(P_{\mathrm{t}}|S_{21}|^2)^3}{L^3 OIP_{3,\mathrm{r}}^2} \tag{7}$$

where P_{N} is the noise power, L is attenuation before the receiver, $|S_{21}|$ is the coupling between the transmitter and receiver, and $OIP_{3,\mathrm{t}}$ and $OIP_{3,\mathrm{r}}$ are the third-order intercept points of the transmitter and the receiver [8].

The response is proportional to the fourth power of the gain. While this is a disadvantage in regards to the dynamic range of the measurement, it is also beneficial. The effect of uncertainty is smaller in gain measurements because the gain then depends on the fourth root of the response.

Noise is constant, but its effect depends on the level of the measured response, which is why we consider it in this section. The total received intermodulation response consists of the transponder response from (1), noise, and the inferference from (7). When the SINR is low, the interference will degrade the measurement result, as illustrated at specific angles in Fig. 2. In the next section, we will estimate the magnitude of this effect.

Noise is incoherent so the powers can be summed. Distortion is coherent so the voltages need to be summed. The measured response P_{r} is

$$P_{\mathrm{r}} = \left(\sqrt{P_{\mathrm{r,tag}}} + \sqrt{P_{\mathrm{I}}}\right)^2 + P_{\mathrm{N}} \tag{8}$$

where $P_{\mathrm{r,tag}}$ is the actual response from the tag, P_{I} is the interference power and P_{N} is the noise power. Here we assume the worst-case scenario where all the sources of interference contribute constructively.

IV. Calculated Measurement Uncertainty

In this section, we will calculate the total uncertainty for the measurement result shown in Fig. 2. The *H*-plane pattern is omnidirectional so we only need to consider the static and power-dependent variables. For the *E*-plane pattern, the angle-dependent variables also need to be considered.

Because of the complicated nature of the gain calculation formulating an analytic solution is difficult. Instead, we incorporate the uncertainties in the model used to calculate the gain

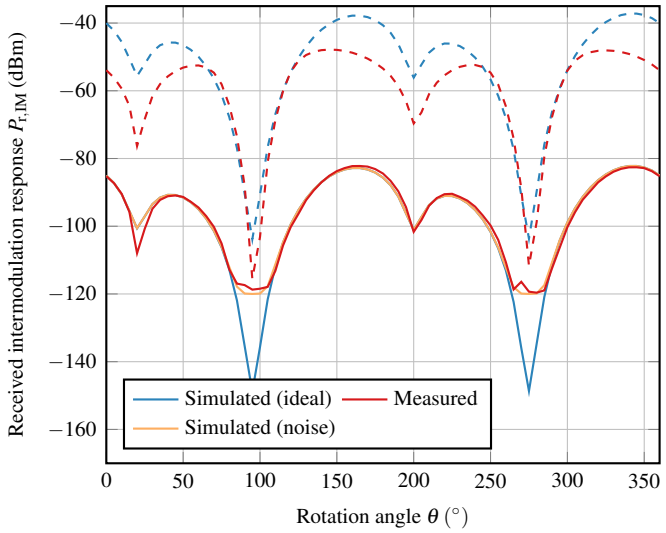

Fig. 4. Comparison of the measured and simulated (noisy and ideal) responses when $P_t = -20$ dBm (solid curves) and $P_t = -5$ dBm (dashed curves).

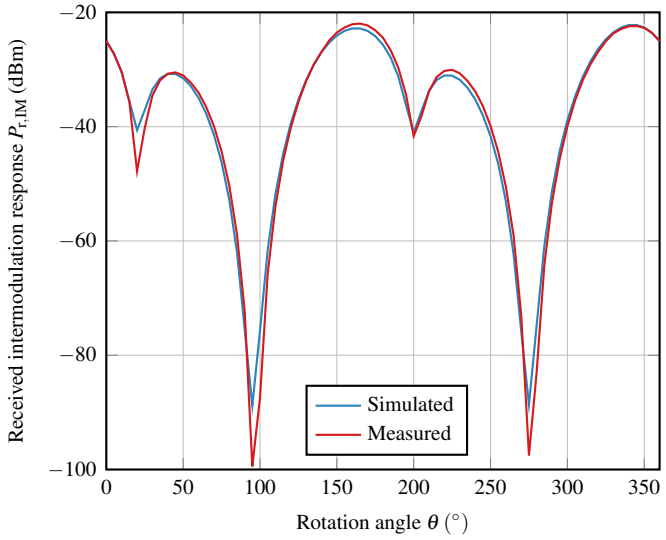

Fig. 5. Comparison of the measured and simulated (noisy and ideal) responses. The result shown includes the iterative power compensation, which removes the effect of the noise completely.

and calculate the two extreme values on the both sides of the measured value.

Fig. 4 illustrates the measured response when the transmit power is -20 dBm. It can be seen that at such power levels, the noise floor of the measurement disturbs the measurement. This can be modelled by summing a noise power of -120 dBm to the simulated model using (8). At higher power levels, e.g. -5 dBm, noise has no effect on the result. Instead, the small-signal model becomes inaccurate and the measured response. The model cannot account for these effects.

Fig. 5 shows the simulated and measured responses after iterative input power compensation. In this technique we adjust the input power at each measurement point based on the

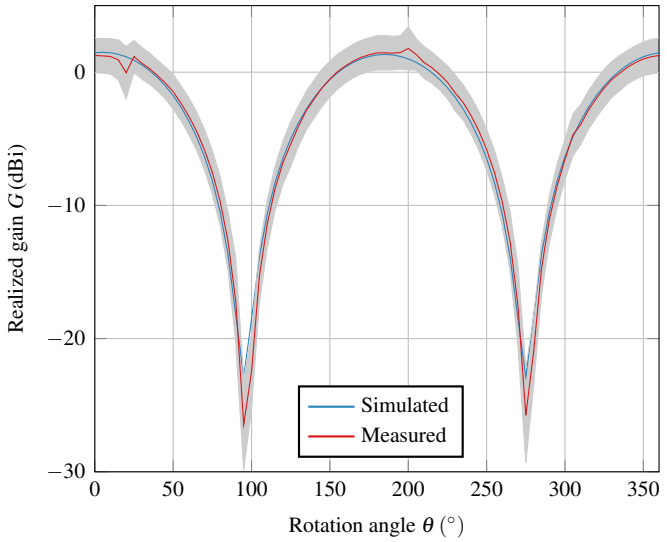

Fig. 6. The measured and simulated E-plane pattern of the harmonic transponder. The measurement uncertainty is represented by the gray area around the measured result.

previously calculated gain value. By including the gain compensation, the effects of the interference and the nonlinearity can be reduced significantly. The ideal and noise-including models do not have any significant differences.

However, the difference between the measurement and the simulation at 20° still remains. Based on the simulations and the geometry of the antenna, we expected the result to be the same at measurement points that are separated by 180°. Because the response at 20° and 200° differs by over 7 dB, there must have been some kind of problem in the measurement setup. The most likely culprit is a slightly mismatched alignment of the antenna. The difference occurs when the null of the AUT is pointed towards the receiver. The gain of the AUT changes rapidly near the null, so a small misalignment can cause the measured gain to change.

Based on this experimental information, we then calculate the uncertainty for the performed measurement. We estimate the uncertainty of all the parameters in (1) and then calculate the gain for the two extreme values of $A + P_r$. The uncertainty of possible misalignment is modelled by estimating the derivative of the received response of P_r as a function of rotation angle. Fig. 6 illustrates the result. We can see that the simulated and measured result agree within the calculated uncertainty value. The H-plane pattern is not shown due to it being omnidirectional. The gain in the H-plane is measured to be 1.45 dBi with an uncertainty of ± 1.27 dB.

V. Conclusion

In this paper, we have analyzed the uncertainty of the intermodulation measurement technique which has been used to characterize the realized gain of a harmonic transponder. We have taken a detailed look at the effect of various uncertainties on the measurement to provide more insight on the

measurement accuracy of this technique. The measurement results were found to be consistent with the simulated values.

The limited dynamic range remains a problem with the measurement technique. This is further complicated by the fact that the AUT should be placed in the far field of the measurement antennas. Both the distance and the received power should be maximized, but this is obviously impossible. A good compromise should therefore be found.

A disadvantage of the bistatic measurement geometry is that the measurement errors from the near the nulls of the antenna pattern also affect the result near the maxima of the pattern. Unlike originally assumed, the SINR is not the only factor contributing to these errors. The measurement result appears to be very sensitive to the alignment of the antenna, especially when the gain changes rapidly.

REFERENCES

[1] K. Finkenzeller, *RFID Handbook*, 3rd ed. John Wiley & Sons, Jun. 2010. [Online]. Available: http://dx.doi.org/10.1002/9780470665121

[2] K. Rasilainen and V. Viikari, "Transponder designs for harmonic radar applications," *International Journal of Antennas and Propagation*, vol. 2015, p. 9, 2015.

[3] V. Viikari, H. Seppä, and D.-W. Kim, "Intermodulation read-out principle for passive wireless sensors," *IEEE Transactions on Microwave Theory and Techniques*, vol. 59, no. 4, pp. 1025–1031, Apr. 2011.

[4] O. Staub, J.-F. Zürcher, and A. Skrivervik, "Some considerations on the correct measurement of the gain and bandwidth of electrically small antennas," *Microwave and Optical Technology Letters*, vol. 17, no. 3, pp. 156–160, Feb. 1998.

[5] C. Icheln and P. Vainikainen, "Dual-frequency balun to decrease influence of RF feed cables in small antenna measurements," *Electronics Letters*, vol. 36, no. 21, pp. 1760–1761, Oct. 2000.

[6] C. Icheln, J. Krogerus, and P. Vainikainen, "Use of balun chokes in small-antenna radiation measurements," *IEEE Transactions on Instrumentation and Measurement*, vol. 53, no. 2, pp. 498–506, Apr. 2004.

[7] M. Ritamäki, A. Ruhanen, V. Kukko, J. Miettinen, and L. H. Turner, "Contactless radiation pattern measurement method for UHF RFID transponders," *Electronics Letters*, vol. 41, no. 13, pp. 723–724, Jun. 2005.

[8] J.-M. Hannula, K. Rasilainen, and V. Viikari, "Characterization of transponder antennas using intermodulation response," *IEEE Transactions on Antennas and Propagation*, vol. 63, no. 6, pp. 2412–2420, Jun. 2015.

[9] C. Icheln, "Methods for measuring RF radiation properties of small antennas," Doctoral dissertation, Helsinki University of Technology, 2001.

[10] J. R. Riley and A. D. Smith, "Design considerations for an harmonic radar to investigate the flight of insects at low altitude," *Computers and Electronics in Agriculture*, vol. 35, no. 2-3, pp. 151–169, Aug. 2002.

[11] K. Rasilainen, J. Ilvonen, A. Lehtovuori, J.-M. Hannula, and V. Viikari, "On design and evaluation of harmonic transponders," *IEEE Transactions on Antennas and Propagation*, vol. 63, no. 1, pp. 15–23, Jan. 2015.